Available online at www.sciencedirect.com

ScienceDirect

journal homepage: www.elsevier.com/locate/he

Microwave assisted synthesis of silver nanoparticles and its application in sustainable photocatalytic hydrogen evolution

Guilherme B. Strapasson [a], *Marcelo Assis* [b], *Cláudio W. Backes* [a], *Silma A. Corrêa* [a], *Elson Longo* [b], *Daniel E. Weibel* [a,*]

[a] *Institute of Chemistry, Universidade Federal do Rio Grande do Sul-UFRGS, Avenida Bento Gonçalves 9500, 91501-970 Porto Alegre, RS, Brazil*

[b] *CDMF, Federal University of São Carlos - UFSCar, P.O. Box 676, 13565–905, São Carlos, São Paulo, Brazil*

HIGHLIGHTS

- Glycerol, Starch and Ag were used for the Microwave synthesis of TiO2@AgNPs.
- Highly stable Ag NPs with diameters from 2.9 nm were prepared.
- Typical steady state photocatalytic H_2 evolution was obtained.
- Sustainable and green hydrogen photoreforming can be achieved.

GRAPHICAL ABSTRACT

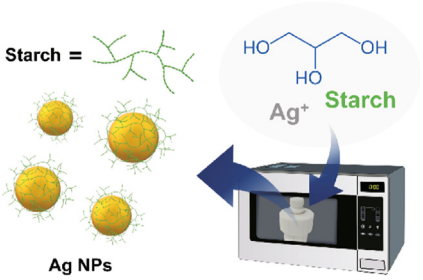

ARTICLE INFO

Article history:
Received 16 May 2021
Received in revised form
4 July 2021
Accepted 31 July 2021
Available online 1 September 2021

Keywords:
Photocatalytic H_2 production
Glycerol
Sustainable synthesis
Microwave irradiation

ABSTRACT

Large amounts of photocatalysts are needed for the generation of solar hydrogen (H_2) and eco-friendly synthetic alternatives are essential. Here, we use glycerol as solvent and reducing agent, and food grade corn starch as stabilizing agent for the preparation of silver nanoparticles (Ag NPs) by microwave irradiation. The Ag NPs were also synthesized using various proportions of glycerol/water mixtures. The Ag NPs were loaded onto commercial TiO_2 NPs to study the photogeneration of H_2. Characterization was carried out by UV–vis, XRD, TEM, UV–Vis DRS, and RBS. Stable Ag NPs after 320 days of aging with diameters from 2.9 to ~44 nm were prepared under several experimental conditions. Finally, TiO_2@AgNPs showed that the rate of evolved H_2 is stable, much higher than pure TiO_2 NPs and proportional to the amount of Ag NPs loaded. The present study introduces a new sustainable and eco-friendly strategy for designing low-cost photocatalysts for H_2 generation.

* *Corresponding author.*
E-mail address: danielw@iq.ufrgs.br (D.E. Weibel).

https://doi.org/10.1016/j.ijhydene.2021.07.237

Introduction

The world's growing energy need, alongside the increasing population led to the continual use of fossil fuel-based energy sources. Environmental concerns have encouraged a constant search for renewable energy sources, such as biomass, that can be converted into liquid fuels (biofuels). Biodiesel, a renewable biofuel, is attracting attention as a clean energetic alternative which does not depend on fossil fuels. It lacks toxicity, sulphured or aromatic by-products and has a relatively low cost [1]. Among biodiesels, glycerol is usually obtained in large amounts as a by-product. It is estimated that 10 kg of glycerol are generated during the production of 100 kg of biodiesel [2]. Agricultural production accounts for a significant portion of the gross domestic product (GDP) in Brazil and the addition of biodiesel to diesel of petrochemical origin was established by law [3]. The amount of biodiesel was increasing from that time and it is foreseen that by 2023 the percentage of biodiesel in the diesel will reach about 15%, rising proportionally to the amount of glycerol generation. The importance of biodiesel and glycerol in Brazil led research groups to investigate with success the biohydrogen production by photo fermentation, using glycerol derived from the production of biodiesel and waste cooking oils [4].

Photocatalytic hydrogen (H_2) is been considered the next-generation energy carrier due to its sustainability and no pollution to the environment. In the last two decades H_2 production induced by photons was extensively studied, but in spite of all the efforts the development of a commercial application is lacking mainly due to the low efficiency and durability of the photocatalysts [5]. Photocatalytic H_2 generation from water splitting [6], photo-reform of alcohols [7], and addition of sacrificial donors [8] represent some examples of the attempts to find an efficient and clean source of H_2 using light as excitation source. This promising green H_2 is based on the use of nanostructured photocatalysts with the addition in many cases of co-catalysts, such as nanoparticles (NPs) or quantum dots. Those small particles increase the photon-hydrogen conversion efficiency by the known plasmon mechanisms: hot electron transfer or local electric field enhancement (optical antenna effect) [9]. The use of metals or noble metals NPs with large work functions lead to electron traps, which favours H_2 evolution [7,10–16]. Additionally, new interesting approaches using several types of photocatalysts were recently reported with the objective to produce photocatalytic H_2, such as Mo–S–P hetrojunction photocatalyst [17], 3D MoS_x nanoflowers [18], MoO_3/Ag/TiO_2 nanotube (NT) arrays synthesized in-situ after impregnation and annealing with $AgNO_3$ and MoO_3 powders on the NTs [19] and the preparation of TiO_2 thin films with Ag_2S NPs grown electronically for a photoelectrochemical water spitting application [20].

Ciamician, G. called our attention more than a century ago, by saying that coal is not inexhaustible and additionally he calculated the daily solar energy that the Sahara desert receives every single day [21]. From that date on, reports are periodically published estimating the desired photocatalyst properties for a commercial solar H_2 system. The main common required parameters are: energy conversion efficiency (between 10% [22–24] and 15% [25]), daily H_2 rate production (from ~10^{-3} g/s m^2 [23] to ~ 0.7 g/s m^2 [22]; in the first calculation it was included the sunlight-angle correction), useful wavelength of light ($400 < \lambda < 800$ nm) [22–25] and durability of the photocatalyst (between 1 year [25] and 10 years [23,24]). The amount of water that would be required to satisfy one-third of the projected energy demand of human society in 2050 using solar energy was also calculated (5.1 10^7 T/day [23]). The above impressive numbers also show that for a practical system, huge amounts of nanostructured photocatalysts and co-catalysts will be needed.

It is important to point out that the traditional synthesis of NPs in many fields and, in particular in the photocatalytic generation of H_2, are not environmentally friendly. In general, the NPs preparation involves harmful synthetic methods, the use of toxic reagents and the generation, in many cases, of dangerous waste. Therefore, some research groups have started to synthesize NPs by green methods, following the concepts of sustainability and green chemistry [26,27]. In recent years, several reports have shown the success in the use of the green precepts for the NPs synthesis [28]. For example, Ag NPs have been prepared using an aqueous extract from *Rosa santana* petals [29], aqueous leaf extract of *Melia azedarach* [30], corn starch and sodium citrate [31], different starch types that act as reducing agents [32], cauliflower waste extract [33] and also employing the extract of a native tree of Central and South America, popularly called "ipê-roxo" in Brazil [34]. Preparation of Au NPs were also reported employing an aqueous rhizome extract of a medicinal plant [35] and glycerol as reducing and stabilizing specie [36]. The green method is not only focused on noble metal NPs synthesis, but also in oxides and other complex nanostructures, such as $SrMnO_3$ NPs [37], $Ce_{0.2}Ni_{0.8}Fe_2O_4$ nanoflakes [38], manganese zinc ferrite NPs [39], and several metal oxide NPs [40]. In almost all the above mentioned examples, the use of microwave irradiation as a conventional synthetic chemistry tool [26] is evident, with some exceptions in the use of ultrasound [34,37].

Several reports were published recently employing glycerol for the production of hydrogen, such as the glycerol reforming using Cu/TiO_2/rGO photocatalysts with various Cu and graphene loadings [14], impregnation of TiO_2, Pd and Pt onto mesoporous γ-Al_2O_3 (catalyst/support) produced from aluminium foil waste [13], an integrated biosystem using crude glycerol and photo-fermentation to produce hydrogen [4] and $LaCoO_3$ perovskite doped with Au, Ag, Cu, Pt for the investigation of the glycerol steam reforming reaction in the temperature range of 400 e 700 °C [48]. In spite of the above recent reports that make use of the eco-friendly glycerol for the production of hydrogen, the use of extensive chemicals in many synthetic steps led them to a deviation of the precepts of sustainability. In the past, we have produced efficient photocatalytic nanostructures using toxic chemical routes with the generation, in many cases, of dangerous waste [7,12,41–44]. Recently our research group shifted to green methods to produce NPs with photocatalytic properties [45]. The aim of this study was the green synthesis of Ag NPs using an eco-friendly alternative: glycerol employed as solvent and reducing agent and food grade corn starch as the stabilizing agent. In the biodiesel production the high miscibility of glycerol with water leads to the generation of glycerol with

about 20% of water [46,47]. For that reason, it was also an important target of the present work to investigate the effect of water in the synthesis of the Ag NPs. Microwave assisted chemistry (MWAC) was chosen as a green source of heating. The nanostructures were characterized by UV–vis spectroscopy, X-ray diffraction (XRD), transmission electron microscopy (TEM), UV–Vis diffuse reflectance spectroscopy (UV–Vis DRS), and Rutherford Backscattering Spectrometry (RBS). Furthermore, the prepared Ag NPs were impregnated onto commercial TiO_2 NPs and tested for the H_2 evolution in the photo-reform of methanol at room temperature. The results presented here show that green synthetic methods can be used efficiently for the preparation of photocatalysts that produce stable H_2 generation by UV–vis light irradiation.

Experimental section

Materials

Silver nitrate ($AgNO_3$) was purchased from Plat LAB (Comércio de Artigos para Laboratórios e Serviços Ltda). Ethanol, methanol and bi-distilled glycerol were purchased from Casa da Química. Titanium dioxide NPs powder, AEROXIDE® TiO_2–P25 from EVONIK (a mixture of about 75% anatase and 25% rutile) was received from Degussa Corporation. Food grade corn starch (Maizena®, Garanhuns/PE – Brazil) was used as received.

Silver nanoparticles syntheses

Silver nanoparticles (Ag NPs) were synthesized by microwave irradiation using pure glycerol as solvent and reducing agent. Food grade corn starch was used as stabilizing agent. A series of runs were also carried out adding water to the mixtures at constant starch/Ag ratio (w/w). A simplified scheme for the syntheses is presented on Scheme 1. For the syntheses using pure glycerol, $AgNO_3$ was solubilised on glycerol, stirred and sonicated for 30 min; then corn starch was added into the mixtures, stirred and sonicated for more 40 min until its complete dispersion; finally, the mixtures were introduced into a homemade Teflon reactor and irradiated at high power for 30 s, using a commercial Panasonic Microwave oven (1600 W of maximum power). The syntheses using glycerol/water mixtures were done with a similar procedure, but water was introduced into the mixtures after corn starch dispersion and sonicated for additional 10 min. All the syntheses were carried out with a final volume of 30 mL. Finally, the mixtures were introduced into the Teflon reactor and irradiated at high power for 30 s, using the same equipment as before. The water percent concentration was varied from 5 to 40% (v/v). The time of 30 s was chosen following previous experiments using the same microwave oven [45].

The synthesized Ag NPs were used to impregnate the commercial TiO_2 NPs (AEROXIDE® TiO_2–P25) by conventional wet impregnation method. For this, Ag NPs were dispersed on ethanol and centrifuged for 10 min at 4000 rpm. Then the supernatant was removed, the Ag NPs were resuspended on water and the TiO_2 NPs were mixed in the suspension with the desired amount of Ag NPs (1.25, 2.50 or 5.00 Ag/TiO_2 wt.%). Finally, the suspension was sonicated for 30 min, oven dried at 80 °C for 24 h and thermal treated at 400 °C in air for 3 h with a heating rate of 3 °C.min^{-1}. The H_2 evolution experiments were carried out impregnating the TiO_2 NPs with Ag NPs prepared using $AgNO_3$ with a concentration of 3 mmol L^{-1}, 10 g L^{-1} of starch and 15% of H_2O. This sample was chosen due to the λ_{max} of the surface plasmon resonance (SPR) as well as the FWHM were the smaller values measured. Additionally, the TEM data confirmed a mean size distribution of the Ag NPs of ~3 nm in diameter (see section Results and discussion).

Characterization

To follow the formation of Ag NPs and to investigate the mean size distribution and stability over time, UV–vis spectroscopy studies were performed on the colloidal Ag NPs, using a CARY 50 spectrophotometer (Varian) in the wavelength range of 200–800 nm.

The crystallographic planes identification of the Ag NPs was conducted with X-ray diffraction using a Siemens Goniometer D500 equipped with Cu Kα radiation at 40 kV and 20 mA. The data were collected for scattering angles (2θ)

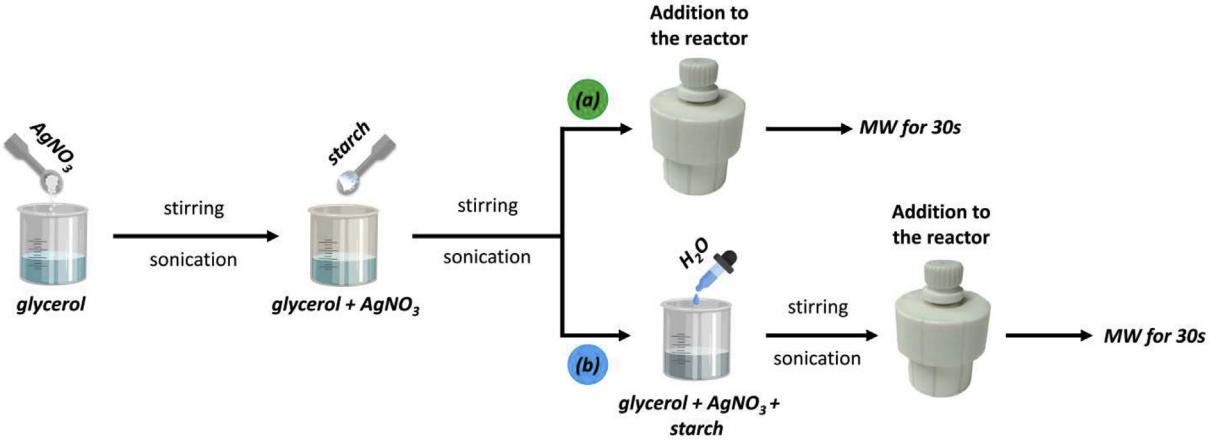

Scheme 1 – Schematic representation for the syntheses of Ag NPs, where the solvent is (a) pure glycerol and (b) glycerol/water mixtures. MW: microwave.

ranging from 20° to 80° with a step size of 0.05°. The results were analysed using the Crystallographica Search-Match (CSM) software.

Transmission electron microscopy (TEM) were performed with a FEI TECNAI F20 (Netherlands) microscope operating at 200 kV. The samples were prepared by depositing small amounts of the Ag NPs solution directly onto holed carbon coated Cu grids. The mean size of the NPs was measured using the software ImageJ®.

The optical properties of the TiO_2 and TiO_2 impregnated NPs with Ag NPs (TiO_2@Ag NPs) were measured using a double-beam CARY 5000 spectrophotometer (Varian) in the wavelength range of 200–800 nm. The bandgap values of samples were determined by UV–Vis measurements with an integrated sphere. The Kubelka–Munk model was used to determine the band-gap assuming that the sample scattering coefficient was constant for the UV–Vis wavelength range.

The Ag/Ti atomic ratios were determined by Rutherford backscattering spectrometry (RBS). The dry TiO_2@Ag NPs were suspended in ethanol and samples were prepared by drop casting the diluted solution on silicon wafers. The analyses were performed using a He^+ ion beam with an incident energy of 2.0 MeV produced by 3 MV Tandetron accelerator. In all measurements, the incident beam was perpendicular to the sample surface and the detection angle was 165° related to the beam direction. Backscattered ions were detected by a semiconductor surface barrier detector and the SIMNRA software [49] was used to evaluate the sample composition by fitting the individual elemental fractions until a good agreement between experimental and calculated data was achieved. The atomic ratios determined were then converted into Ag/TiO_2 weight percentage (wt. %) by using each element respective atomic weight.

Photocatalytic hydrogen measurements

Hydrogen photogeneration experiments were carried out using a calibrated (24.16 ± 0.01) mL gas-closed photochemical reactor made of PTFE under continuous magnetic stirring. A quartz window of 2.54 cm in diameter allowed irradiation of the samples under a wide incident spectral range, including UV and visible light. Typically, 1 mg mL^{-1} of each photocatalyst was suspended on a methanol/water solution (~1/8 v/v) and sonicated for 30 min. The ratio of methanol/water solution of about 1/8 v/v was a typical ratio used in our previous works where different experimental conditions were already studied. Prior to irradiation, the reactor was deaerated with nitrogen during 20 min. The photocatalysis was carried out with a high pressure Xe/Hg lamp of 350 W (Scientech), and the photocatalytic activity was evaluated by gas chromatography (Shimatzsu GC-2010 chromatograph) using a molecular sieve 5 A packed column following a previously reported procedure [7,12].

Results and discussion

Ag nanoparticles synthesis and characterization

Silver nanoparticles (Ag NPs) were synthesized by microwave irradiation using $AgNO_3$ as silver precursor, pure glycerol as solvent and reducing agent, together with the addition of food grade corn starch as stabilizing agent. The optical absorption spectra obtained after the syntheses (Fig. 1) show a strong absorption in the visible region at about 405–420 nm, for all samples. Those absorptions are mainly originated from the well-known surface plasmon resonance (SPR) effect of the Ag NPs [50]. A dependence of the λ_{max} (wavelength at the maximum absorption) and the FWHM (Full Width at Half Maximum) on the $AgNO_3$ and starch concentrations can also be observed (Fig. 1). A continuous decrease in λ_{max} and FWHM can be clearly seen when the concentration of starch increases (Fig. S1. ESI). If the concentration of starch is equal to or greater than 20 g L^{-1} a limit value was obtained in all the cases studied. The λ_{max} reached (407 ± 2) nm and the FWHM stabilized in (65 ± 11) nm (Fig. S1. ESI). Those values were almost independent of the $AgNO_3$ concentration employed on the syntheses. Those results may indicate that with the increase of starch concentration the Ag NPs mean size became smaller and with a narrower size distribution (Fig. S1. ESI).

Conventionally, the first step for the glycerol-rich treatment process consists on the removal of non-volatile components using filtration, ion exchange resins, and activated carbon adsorption. The second step generally involves high-energy cost evaporation, which removes the major volatile components. The material stream obtained in the second treatment step is mainly composed of glycerol (>80%) and water [46]. For that reason, several runs were carried out to know if it would be possible to prepare Ag NPs also in the presence of water. The optical absorption spectra obtained for the syntheses using glycerol/water mixtures show immediately the merge of the characteristic SPR effect of the Ag NPs (Fig. 2). Keeping the concentrations of $AgNO_3$ and starch constant, the %H_2O was varied from 0 to 40%. It is observed that the maximum in the SPR intensity occurs at about 15% of H_2O (v/v) (Fig. 2-inset). Furthermore, the λ_{max} of absorption when the amount of H_2O was 10–15% (v/v) corresponded to a wavelength of 403 nm, slightly lower than without water addition (Fig. S1. ESI). When the amount of water was <10% (v/v) or > 15% (v/v), the λ_{max} of absorption always increased (Table S1. ESI). The FWHM strongly increased at a H_2O content higher than 15% (v/v) (Table S1. ESI). These results indicate that Ag NPs can potentially be prepared successfully using a green method even in the presence of water. It means that in the production of biodiesel the secondary product, i.e. glycerol, and water (<20%) can be directly employed to produce Ag NPs without any further purification step in the glycerol/water separation process.

Typical XRD diffractograms of Ag NPs synthesized using 3 mmol L^{-1} of $AgNO_3$ and 10 g L^{-1} of starch, on a glycerol/water mixture (Fig. 3a) and on pure glycerol (Fig. 3b), show the characteristic pattern of metallic silver. The prepared Ag NPs possessed good crystallinity and high purity with four signals in the range of $2\theta = 37.5°–77.5°$ that can be assigned as (111), (200), (220), and (311) planes, respectively, corresponding to face centred cubic (fcc) silver crystal structure. The broad peak centred at $2\theta = 24°$ corresponds to the glass substrate used in the measurements [51].

To examine the particle morphology under the several synthesis conditions used, TEM analyses were performed. Typical TEM images of the Ag NPs prepared by microwave

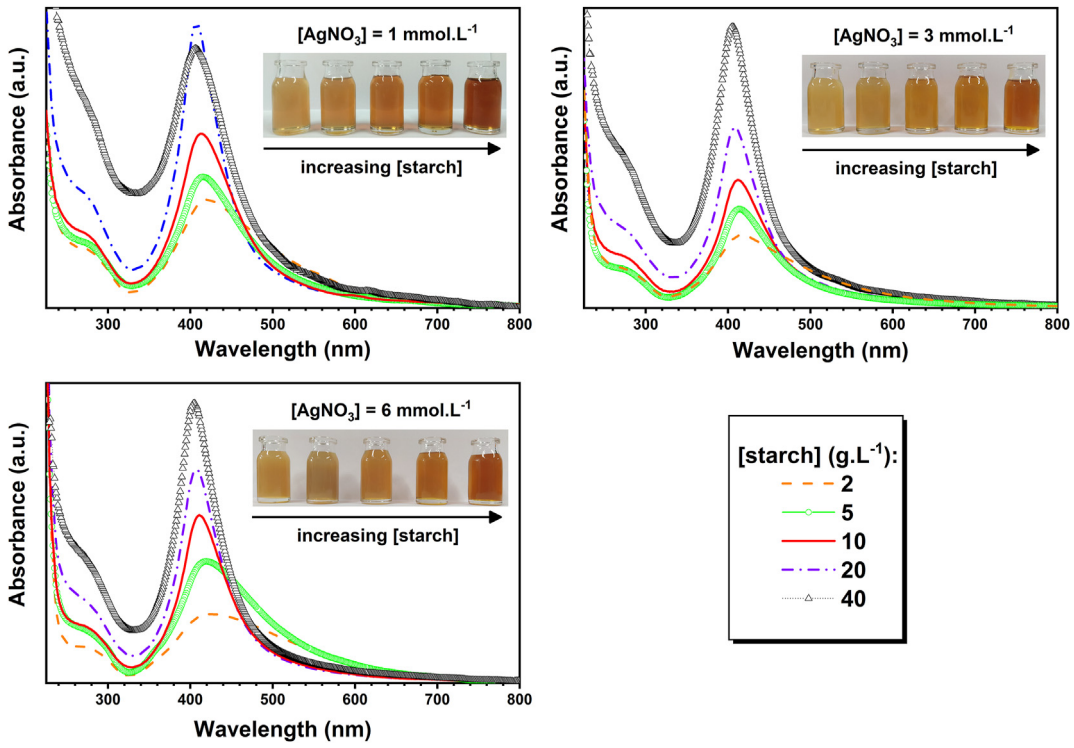

Fig. 1 – UV–Vis absorbance spectra of Ag NPs obtained from optimized synthesis at several $AgNO_3$ and food grade corn starch concentrations. The insets show the photo of the solutions after microwave irradiation.

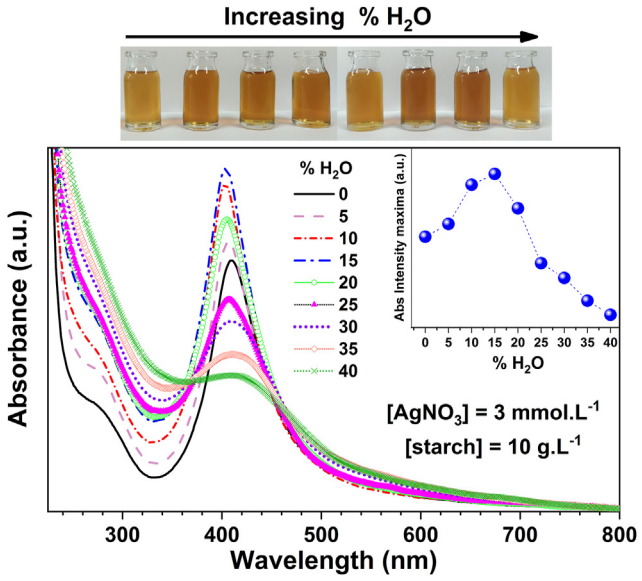

Fig. 2 – UV–Vis absorbance spectra of Ag NPs prepared from optimized synthesis by microwave irradiation with several additions of H_2O (% v/v). The concentrations of $AgNO_3$ and food grade corn starch are indicated in the figure. The photo shows the colours of the solutions after microwave irradiation with increasing H_2O concentration. The inset shows the change in the λ_{max} intensity as a function of the H_2O increase (% v/v). (For interpretation of the references to color in this figure legend, the reader is referred to the Web version of this article).

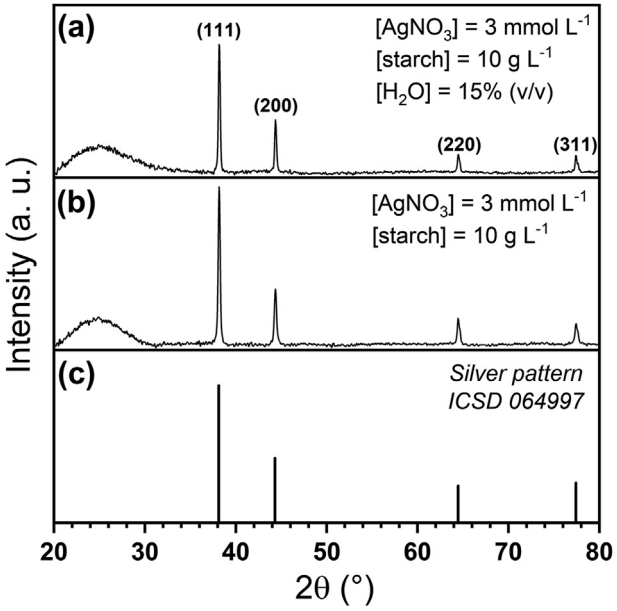

Fig. 3 – XRD pattern of: (a) silver nanoparticles prepared by microwave irradiation from $AgNO_3$ (3 mmol L^{-1}) in the presence of food grade corn starch (10 gL^{-1}) on glycerol/water mixture (15% H_2O v/v); (b) Same as (a) but on pure glycerol; (c) Silver pattern of fcc crystal structure (ICSD 064997).

irradiation from 1 mmol L^{-1} $AgNO_3$ on pure glycerol and 20 g L^{-1} of starch showed the existence of circular nanoparticles with mean diameter of (10.7 ± 3.9) nm (Fig. 4a–c and Table 1). When the amounts of $AgNO_3$ increased to 3 mmol L^{-1} the Ag NPs mean diameter slightly increased to (15.9 ± 4.0) nm (Fig. 4d–f and Table 1). Increasing the concentration of $AgNO_3$ and starch even more, to 6 mmol L^{-1} and 40 g L^{-1}, respectively (Fig. 4g–i), no remarkable changes in the mean size (11.5 ± 6.9 nm) of the Ag NPs were observed (Table 1). If water was added to the synthesis the mean diameters of Ag NPs (2.9 ± 1.4 nm) agree with the information obtained by optical absorption spectroscopy where a minimum value of λ_{max} and FWHM was measured (Table S1. ESI). Some amounts of larger Ag NPs were also observed, probably due to agglomeration, with a mean diameter of (21.8 ± 8.1) nm (Fig. 4j–l and Table 1).

In some experimental conditions using a low amount of $AgNO_3$ on pure glycerol (1 mmol L^{-1}), without addition of water and 5 or 10 g L^{-1} of starch; a bimodal distribution of the Ag NPs sizes was also observed (Table 1). In those cases, doubling the starch concentration decreased the mean diameter of the Ag NPs by half. As the starch is used as stabilizing agent, it is already known from the classical and modified polyol process that the size and shape of nanostructures depend on the amount of stabilizing used [52,53]. Nevertheless, approximately 90% of the Ag NPs corresponds to the smaller diameter (Fig. S3. ESI and S4. ESI). TEM images and

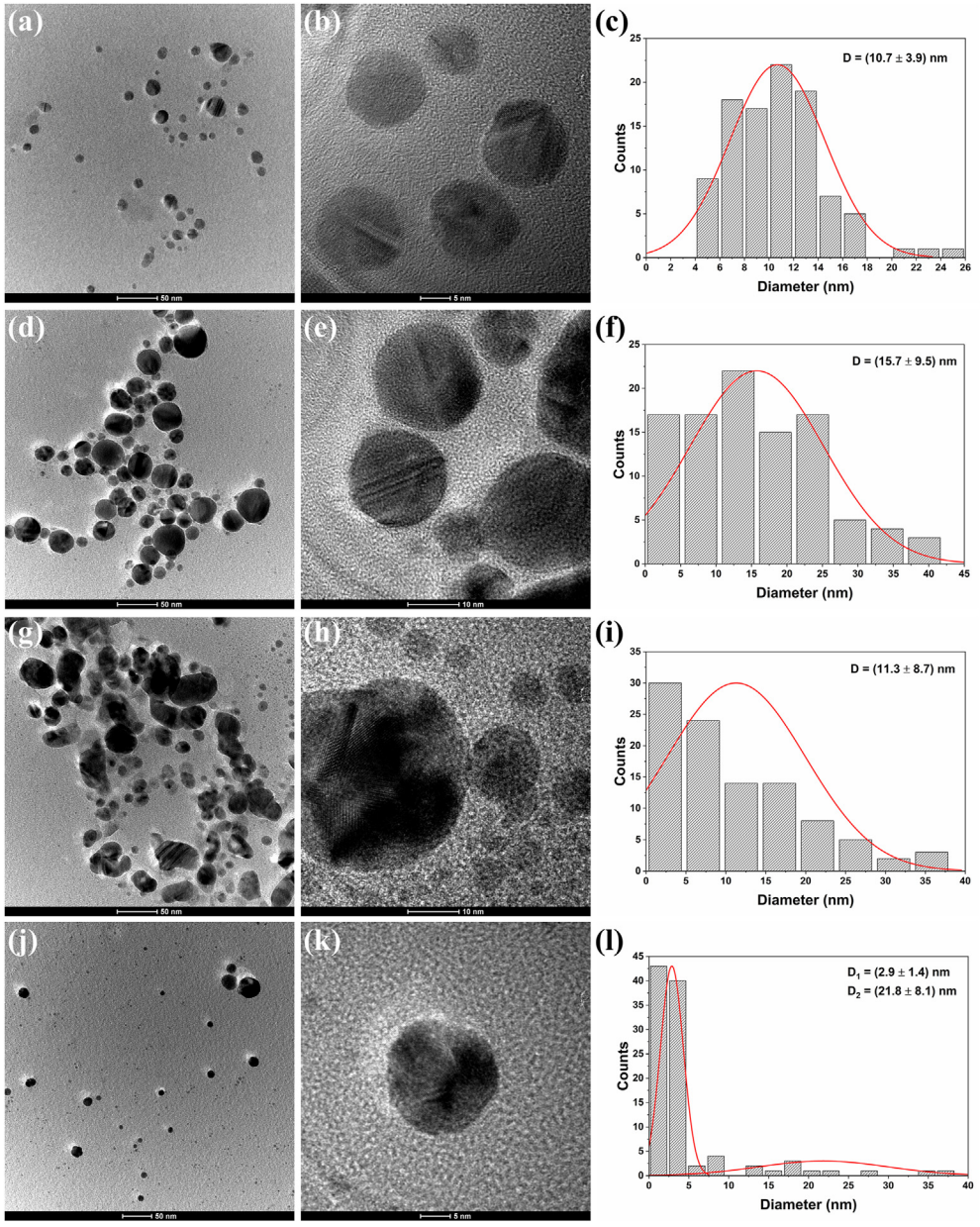

Fig. 4 – TEM image of Ag NPs prepared by microwave irradiation and its size distribution from: (a–c) 1 mmol L^{-1} $AgNO_3$ on pure glycerol and 20 g L^{-1} of starch; (d–f) 3 mmol L^{-1} $AgNO_3$ on pure glycerol and 20 g L^{-1} of starch; (g–i) 6 mmol L^{-1} $AgNO_3$ on pure glycerol and 40 g L^{-1} of starch and (j–l) 3 mmol L^{-1} $AgNO_3$ on glycerol/water mixture (15% of H_2O) and 10 g L^{-1} of starch.

Table 1 – Average calculated diameter of the Ag NPs prepared by microwave irradiation under several experimental conditions. The two values of the average diameter correspond to bimodal distributions. The mean size of the NPs was measured using the software ImageJ®.

[$AgNO_3$] (mmol.L^{-1})	[Starch] (g.L^{-1})	% H_2O (v/v)	Mean size (nm)
1	2	–	39.3 ± 22.5
1	5	–	11.6 ± 5.2
			43.9 ± 11.1
1	10	–	5.4 ± 1.8
			20.2 ± 2.9
1	20	–	10.7 ± 3.9
3	10	–	15.9 ± 4.0
3	20	–	15.7 ± 9.5
3	40	–	11.5 ± 6.9
6	20	–	21.3 ± 6.4
6	40	–	11.3 ± 8.7
3	10	15	2.9 ± 1.4
			21.8 ± 8.1

size distribution histograms from Table 1 samples are presented from Figs. S2–S11 (ESI).

Reproducibility and stability tests of the Ag NPs

It is highly desirable in the preparation of metal NPs, that the syntheses present reproducibility and also have good stability over time. Therefore, a series of runs were carried out to test the reproducibility and aging of the prepared Ag NPs. Three independent preparations of Ag NPs using 3 mmol L^{-1} of $AgNO_3$ dissolved on pure glycerol and 10 g L^{-1} of food grade corn starch led to almost identical results in λ_{max} of absorption, FWHM and intensity (Fig. 5a) showing the high reproducibility of the synthetic method employed. The aging experiments showed a very high stability of the prepared Ag NPs because the aggregation processes did not affect in a great extent the optical properties of the SPR effect of the Ag NPs. In the case of the synthesis of Ag NPs using 3 mmol L^{-1} of $AgNO_3$ on pure glycerol and 10 g L^{-1} of food grade corn starch (Fig. 5b) a shift of about 1.2% of the λ_{max} of absorption was observed after 320 days of aging (from 411 nm to 416 nm) and almost no shift within 30 days of aging was observed. When water was used in the preparation method about 2% shift in the λ_{max} of absorption was measured after 320 days of aging (from 405 nm to 413 nm). Less than 1% shift in the λ_{max} of absorption occurs after 30 days of aging. As it should be expected a probable aggregation process of the NPs is facilitated by the water presence in the liquid medium. Fig. S12 (ESI) shows how the FWHM and λ_{max} evolve for both stability test samples from Fig. 5.

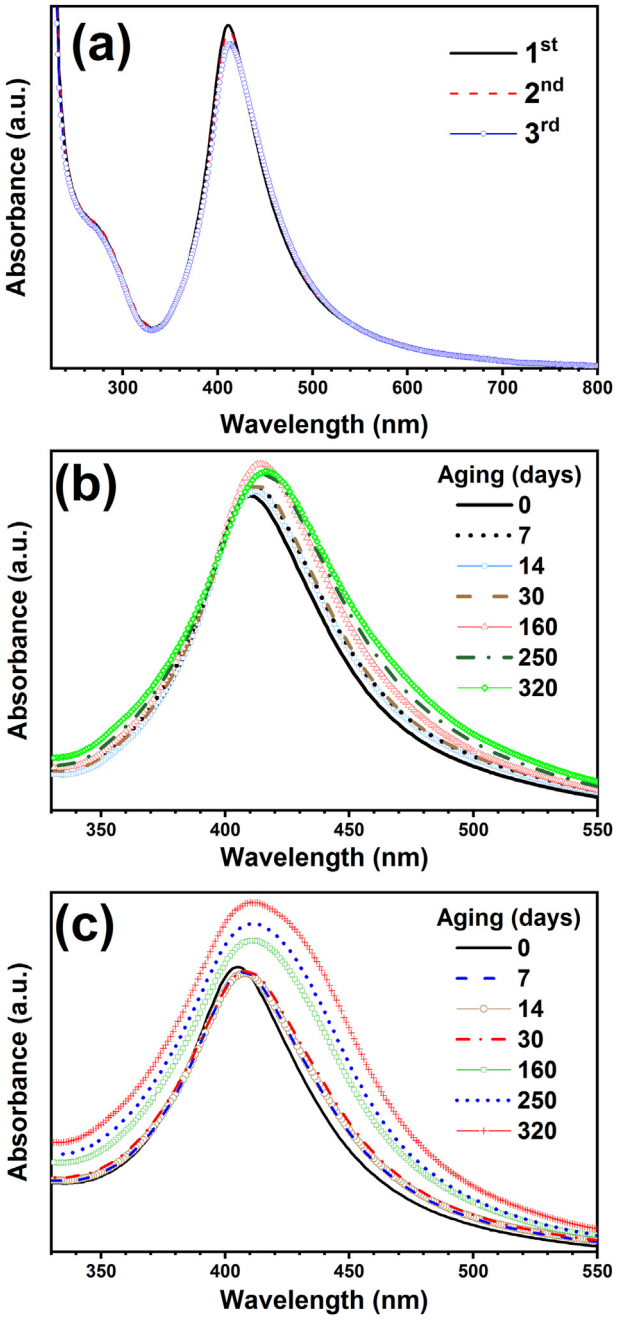

Fig. 5 – Reproducibility and stability tests of the prepared Ag NPs measured by optical absorption spectra. (a) Three independent synthesis of Ag NPs using $AgNO_3$ (3 mmol L^{-1}) on pure glycerol and food grade corn starch (10 g L^{-1}); (b) Aging of Ag NPs prepared in (a); (c) Aging of Ag NPs prepared using glycerol/water mixture and food grade corn starch. [$AgNO_3$]: 3 mmol L^{-1}, [starch]: 10 g L^{-1}, H_2O: 15% (v/v).

Photocatalytic hydrogen generation by impregnation of green Ag NPs on TiO_2 NPs

The prepared Ag NPs were loaded onto a photocatalyst commonly used as reference in the literature, i.e. the TiO_2 NPs (AEROXIDE® TiO_2–P25). The final co-catalyst was further employed for H_2 photogeneration experiments under UV–vis irradiation. UV–Vis diffuse reflectance spectra (DRS) of bare P25 TiO_2 NPs showed the fundamental absorbance edge at about 3.2 eV (Fig. 6a). A shift in the absorption edge towards the visible-light region and the appearance of a noticeable visible band is observed for the Ag NPs-impregnated TiO_2 catalyst (TiO_2@AgNPs) (Fig. 6a). The intensity of the visible

band absorption centred at about 2.5 eV (~496 nm) increased as the Ag NPs amount increased, indicated as Ag/TiO_2 wt.% (Ag/TiO_2 weight ratio percentage) in the figure.

The Rutherford backscattering spectrometry (RBS) technique was employed in order to determine the composition of Ag NPs-impregnated TiO_2 catalyst. RBS measurements can be performed with small amounts of sample material and it can provide quantitative information on elemental composition, depth and thickness of layers in a film with the advantage that typically it does not require the use of standards [54]. The use of RBS in the characterization of catalysts [55,56], photocatalysts [57,58], NPs [59,60], and nanocrystals [61,62] is well documented in the literature. The experimental RBS data of TiO_2@AgNPs samples are shown in Fig. 6b. The four steps seen in Fig. 6b correspond to signals from Ag, Ti, Si, and O, respectively, from the right to the left. The silicon signal in all three samples stands for the substrate on which solutions of the TiO_2@AgNPs were dripped. Moreover, one can clearly see a Fe contamination signal in the P25 + 2.50% Ag sample. This contamination is more likely to come from the impregnation procedure. It was hypothesized that the Fe contamination was accidental and probably the Teflon magnetic stirrer bar during the impregnation procedure had an unseen small damage on it. The sensitivity of RBS on metals depend on the mass and for Fe the technique is highly sensitivity. Nevertheless, to confirm or not the presence of Fe on the surface XPS spectra were acquired. The XPS results for the P25 + 2.50% Ag sample did not show any Fe 2p signal (See Fig. S16 in SI). Therefore, no effect on the photocatalytic results would be expected.

The elemental composition was determined by fitting of the RBS data using the SIMNRA software [49] and results are presented in Table 2 as Ag/TiO_2 wt.%. The fitting for each sample is shown in Figs. S13, S14, S15 (ESI). As revealed by RBS, the amount of Ag NPs that are effectively impregnated in the commercial TiO_2 NPs is less than 30% of the amounts in the corresponding Ag NPs suspension (see Experimental section for details regarding the impregnation procedure). The Ag/TiO_2 wt.% amount determined by RBS for the P25 + 1.25% Ag sample corresponds to only 27% of its nominal amount of 1.25% Ag employed in the impregnation. The amounts impregnated are even lower for the P25 + 2.50% Ag and P25 + 5.00% Ag samples, i.e. 25% and 20%, respectively.

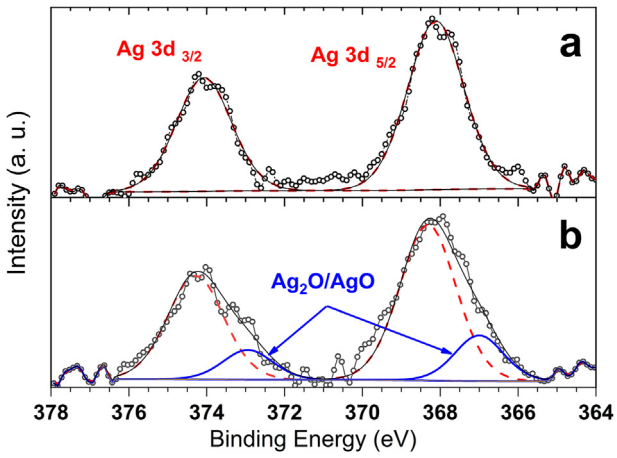

Fig. 7 – Silver 3d regions of XPS spectra after UV–vis irradiation (a) and before irradiation (b). TiO_2 NPs (P25) were impregnated with Ag (5 % wt.). AgNPs were prepared by microwave irradiation. a.u. stands for arbitrary units.

Table 2 – The Ag/TiO_2 wt.% amount as determined by RBS. Normalized H_2 evolution rate is also presented.

Sample[a]	Amount determined by RBS (Ag/TiO_2 wt.%)	Normalized H_2 evolution rate (μmol g^{-1} h^{-1})[b]
P25	0	1
P25 + 1.25% Ag	0.34	3.3
P25 + 2.50% Ag	0.62	4.9
P25 + 5.00% Ag	1.02	7.0

[a] The amount of impregnated Ag NPs is referred in the name of the samples as % Ag.
[b] Data obtained from Fig. 8a.

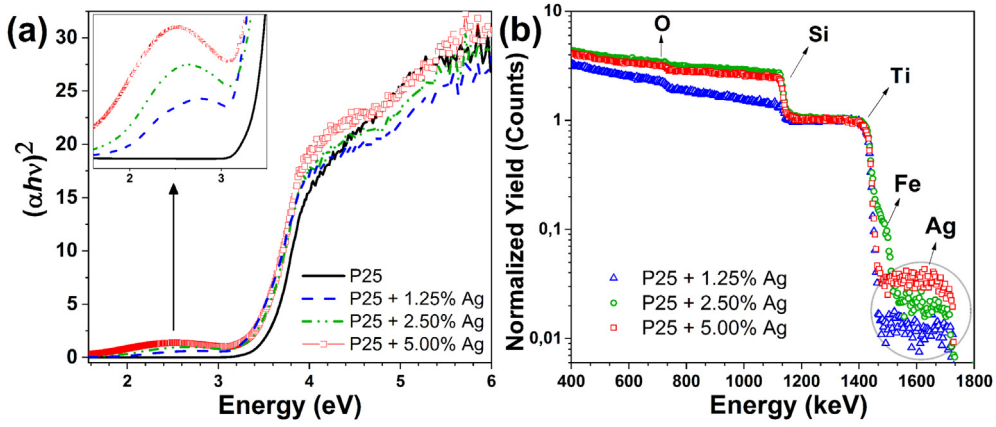

Fig. 6 – The amount of impregnated Ag is shown in the figure as Ag/TiO_2 wt.%. (a) DRS UV–Vis of TiO_2 NPs (P25) and TiO_2 NPs (P25) impregnated with Ag NPs (TiO_2@AgNPs) prepared by microwave irradiation. (b) RBS data of the TiO_2@AgNPs. The backscattered yield was normalized by the Ti signal and logarithmic scale was used to better display the amount of Ag observed for each sample.

XPS spectroscopy was used to confirm the presence of silver on the surface before and after the photocatalytic reactions. The results show in Fig. 7 clearly demonstrate the presence of Ag 3d signals with the Ag $3d_{5/2}$ and Ag $3d_{3/2}$ peaks appearing at 368.2 eV and 374.1 eV, respectively and with 6 eV of the 3d doublet splitting [63]. Fig. 7b also evidences a partial oxidation of the Ag NPs before the photocatalytic reaction (Ag_2O or AgO). Under the actual XPS experimental conditions the expected spectra resolution should be about 1 eV and due to the small binding energy difference between Ag_2O and AgO, the signals cannot be properly separated. The inclusion of the oxidized Ag was necessary because the FWHM (Full Width at High Maximum) before irradiation of the Ag $3d_{5/2}$ and Ag $3d_{3/2}$ signals was ~2.2 eV larger than the actual width of ~1.5–1.7 eV observed, for example, in the irradiated silver co-catalyst (Fig. 7a). The analyses of the O 1s signals did not show important differences between irradiated and non irradiated samples probably due to much higher concentration of TiO_2 than silver (see Fig. S17 in SI).

Reactions using metal oxide semiconductors as photocatalysts for the generation of H_2 are usually carried out in aqueous solutions with the addition of easily oxidizable reducing agents [64,65]. The photogenerated holes irreversibly oxidize those species, such as methanol, instead of water. By this way the electron concentration on the photocatalyst surface increases and the H_2 evolution rate is enhanced. Reactions using sacrificial agents are regarded as half reactions and usually called as photo-induced reforming of alcohols at room temperature. Those types of reactions are very useful in photocatalytic H_2 or O_2 evolution tests. Typical results obtained in the presence of methanol-water solutions on TiO_2@AgNPs show that the rate of evolved H_2 (μmol g^{-1}) is much higher than pure TiO_2 NPs and proportional to the amount of Ag NPs loaded onto the TiO_2 NPs (Fig. 8a and Table 2). Even though the RBS data showed an apparent inefficient impregnation of the TiO_2 NPs (see Table 2), it was enough to observe an increase in the photocatalytic hydrogen production when TiO_2@AgNPs were used as compared to results for TiO_2 commercial P25. The time evolution pattern of hydrogen generation from a mixture of water and methanol under UV–Vis illumination using TiO_2@AgNPs co-catalyst indicated that H_2 production evolved steadily and the photocatalytic activity did not deteriorate, even after 12 h of continuous irradiation (Fig. 8b).

The photocatalytic hydrogen production from aqueous alcohol solutions using TiO_2 photocatalyst with simultaneous noble metal loading was studied and reviewed in the past [16,66–69]. Briefly, the mechanism of SPR coupling with TiO_2@AgNPs using methanol as sacrificial specie for the hydrogen evolution can be explained with the help of the following reactions:

$$TiO_2@AgNPs + h\nu \rightarrow TiO_2@AgNPs\ (e^-_{CB} + h^+_{VB}) \quad (1)$$

The photogenerated holes (h^+_{VB}) migrate to the surface of TiO_2 and oxidize the surface OH groups, water or CH_3OH adsorbed on TiO_2 to produce HO· radicals according to the well known mechanism [12,66]:

$$OH_{surface\ group} + h^+_{VB} \rightarrow HO\cdot \quad (2)$$

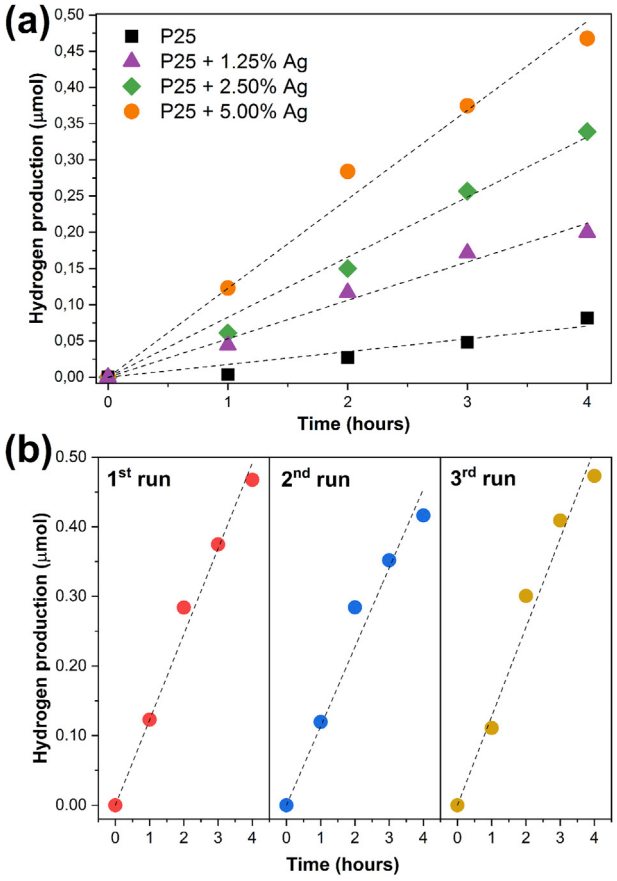

Fig. 8 – (a) Photocatalytic hydrogen production over UV–Vis irradiation using the prepared TiO_2@AgNPs co-catalyst. Methanol was used as sacrificial agent (methanol/water solution: ~1/8 v/v). (b) Typical hydrogen evolution rate showing the stability of the photocatalytic reaction. Photocatalyst: TiO_2 commercial P25 + 5% Ag NPs (Ag:TiO_2 wt.%). Methanol/water solution: ~1/8 v/v.

$$H_2O + h^+_{VB} \rightarrow HO\cdot + H^+ \quad (3)$$

$$CH_3OH + h^+_{VB} \rightarrow CH_3O\cdot + H^+ \quad (4)$$

$$CH_3O\cdot + h^+_{VB} \rightarrow CH_2O\cdot + H^+ \quad (5)$$

$$CH_2O\cdot + h^+_{VB} \rightarrow CHO\cdot + H^+ \quad (6)$$

$$CHO\cdot + \cdot OH \rightarrow HCOOH \quad (7)$$

$$HCOOH + h^+_{VB} \rightarrow HCOO\cdot + H^+ \quad (8)$$

$$HCOO\cdot + h^+_{VB} \rightarrow CO_2 + H^+ \quad (9)$$

On the other side, the fast reactions described above allow methanol to be an efficient hole scavenger and potentially hydrogen atom "reservoirs" at the Ag and TiO_2 interface. The final reduction of H^+ to H atoms leads to molecular hydrogen generation.

Conclusions

Microwave-assisted synthesis of well-crystallized Ag NPs, using glycerol and food grade corn starch has proven to be a fast-green eco-friendly methodology. Under diverse experimental conditions, including the presence of water, Ag NPs were obtained with diameters between 2.9 and ~44 nm. The synthetic method was very reproducible and the prepared Ag NPs were highly stable after 320 days of aging. Furthermore, the Ag NPs were loaded onto commercial TiO_2 NPs. The Ag/TiO_2 wt. % amount determined by RBS for the TiO_2@AgNPs co-catalysts showed that the Ag concentrations varied proportional to the nominal amounts employed in the impregnation from 20% to 27%. The evolved H_2 under UV–Vis irradiation in the presence of methanol-water solutions showed that the H_2 generation rate was much higher than pure TiO_2 NPs and proportional to the amount of Ag NPs loaded onto the TiO_2 NPs. The route for the Ag NPs preparation described in this work can be used for synthesizing various nanoparticles and it shows the potential for photocatalysts preparation in large amounts using sustainable chemical compounds.

Declaration of competing interest

The authors declare that they have no known competing financial interests or personal relationships that could have appeared to influence the work reported in this paper.

Acknowledgements

This work was funded in part by Fundação de Apoio da Universidade Federal do Rio Grande do Sul – FAURGS, Fundação de Amparo à Pesquisa do Estado de São Paulo – FAPESP (FAPESP CEPID-finance code 2013/07296-2), Conselho Nacional de Desenvolvimento Cientifico e Tecnológico – CNPq (finance codes 166281/2017-4 and 402360/2016-8) and Coordenação de Aperfeiçoamento de Pessoal de Nível Superior – CAPES (finance code 001).

Appendix A. Supplementary data

Supplementary data to this article can be found online at https://doi.org/10.1016/j.ijhydene.2021.07.237.

REFERENCES

[1] Gonçalves VLC, Pinto BP, Silva JC, Mota CJA. Acetylation of glycerol catalyzed by different solid acids. Catal Today 2008;133–135:673–7.
[2] Chol CG, Dhabhai R, Dalai AK, Reaney M. Purification of crude glycerol derived from biodiesel production process: experimental studies and techno-economic analyses. Fuel Process Technol 2018;178:78–87.
[3] Mota CJA, da Silva CXA, Gonçalves VLC. Gliceroquímica: novos produtos e processos a partir da glicerina de produção de biodiesel. Quim Nova 2009;32:639–48.
[4] Rodrigues CV, Rios Alcaraz FA, Nespeca MG, Rodrigues AV, Motteran F, Tallarico Adorno MA, et al. Biohydrogen production in an integrated biosystem using crude glycerol from waste cooking oils. Renew Energy 2020;162:701–11.
[5] Rajeshwar K, Thomas A, Janáky C. Photocatalytic activity of inorganic semiconductor surfaces: myths, hype, and reality. J Phys Chem Lett 2015;6:139–47.
[6] Ge M, Cai J, Iocozzia J, Cao C, Huang J, Zhang X, et al. A review of TiO2 nanostructured catalysts for sustainable H2 generation. Int J Hydrogen Energy 2017;42:8418–49.
[7] Languer MP, Scheffer FR, Feil AF, Baptista DL, Migowski P, Machado GJ, et al. Photo-induced reforming of alcohols with improved hydrogen apparent quantum yield on TiO2 nanotubes loaded with ultra-small Pt nanoparticles. Int J Hydrogen Energy 2013;38:14440–50.
[8] Haider Z, Kang YS. Facile preparation of hierarchical TiO2 nano structures: growth mechanism and enhanced photocatalytic H-2 production from water splitting using methanol as a sacrificial reagent. ACS Appl Mater Interfaces 2014;6:10342–52.
[9] Tada H. Overall water splitting and hydrogen peroxide synthesis by gold nanoparticle-based plasmonic photocatalysts. Nanoscale Adv 2019;1:4238–45.
[10] Zhang L, Pan NQ, Lin SW. Influence of Pt deposition on water-splitting hydrogen generation by highly-ordered TiO2 nanotube arrays. Int J Hydrogen Energy 2014;39:13474–80.
[11] Yu JG, Qi LF, Jaroniec M. Hydrogen production by photocatalytic water splitting over Pt/TiO_2 nanosheets with exposed (001) facets. J Phys Chem C 2010;114:13118–25.
[12] Fornari AMD, Araujo MBd, Duarte CB, Machado G, Teixeira SR, Weibel DE. Photocatalytic reforming of aqueous formaldehyde with hydrogen generation over TiO2 nanotubes loaded with Pt or Au nanoparticles. Int J Hydrogen Energy 2016;41:11599–607.
[13] Osman AI, Skillen NC, Robertson PKJ, Rooney DW, Morgan K. Exploring the photocatalytic hydrogen production potential of titania doped with alumina derived from foil waste. Int J Hydrogen Energy 2020;45:34494–502.
[14] Seadira TWP, Masuku CM, Scurrell MS. Solar photocatalytic glycerol reforming for hydrogen production over Ternary Cu/THS/graphene photocatalyst: effect of Cu and graphene loading. Renew Energy 2020;156:84–97.
[15] Zhou X, Jin B, Luo J, Ning X, Zhan L, Xu X, et al. One-pot solvothermal synthesis of 1D plasmonic TiO2@Ag nanorods with enhanced visible-light photocatalytic performance. Int J Hydrogen Energy 2019;44:10585–92.
[16] Gogoi D, Namdeo A, Golder AK, Peela NR. Ag-doped TiO2 photocatalysts with effective charge transfer for highly efficient hydrogen production through water splitting. Int J Hydrogen Energy 2019;45:2729–44.
[17] Zhang L, Hao X, Wang Y, Jin Z, Ma Q. Construction strategy of Mo-S@Mo-P heterojunction formed with in-situ phosphating Mo-S nanospheres toward efficient photocatalytic hydrogen production. Chem Eng J 2020;391:123545.
[18] Yan X, Wang G, Zhang Y, Guo Q, Jin Z. 3D layered nano-flower MoSx anchored with CoP nanoparticles form double proton adsorption site for enhanced photocatalytic hydrogen evolution under visible light driven. Int J Hydrogen Energy 2020;45:2578–92.
[19] Yao Y, Sun M, Zhang Z, Lin X, Gao B, Anandan S, et al. In situ synthesis of MoO3/Ag/TiO2 nanotube arrays for enhancement of visible-light photoelectrochemical performance. Int J Hydrogen Energy 2019;44:9348–58.

[20] Singh SV, Gupta U, Mukherjee B, Pal BN. Role of electronically coupled in situ grown silver sulfides (Ag2S) nanoparticles with TiO2 for the efficient photoelectrochemical H2 evolution. Int J Hydrogen Energy 2020;45:30153–64.
[21] Ciamician G. The photochemistry OF the future. Science 1912;36:385–94.
[22] Bard AJ, Fox MA. Artificial photosynthesis: solar splitting of water to hydrogen and oxygen. Acc Chem Res 1995;28:141–5.
[23] Maeda K. Photocatalytic water splitting using semiconductor particles: history and recent developments. J Photoch Photobio C 2011;12:237–68.
[24] Fujishima A, Rao TN, Tryk DA. Titanium dioxide photocatalysis. J Photoch Photobio C 2000;1:1–21.
[25] Fujishima A, Zhang X, Tryk DA. Heterogeneous photocatalysis: from water photolysis to applications in environmental cleanup. Int J Hydrogen Energy 2007;32:2664–72.
[26] Kharissova OV, Kharisov BI, Gonzalez CMO, Mendez YP, Lopez I. Greener synthesis of chemical compounds and materials. R Soc Open Sci 2019;6:191378.
[27] Cinelli M, Coles SR, Nadagouda MN, Blaszczynski J, Slowinski R, Varma RS, et al. A green chemistry-based classification model for the synthesis of silver nanoparticles. Green Chem 2015;17:2825–39.
[28] Basheer AA, Ali I. Water photo splitting for green hydrogen energy by green nanoparticles. Int J Hydrogen Energy 2019;44:11564–73.
[29] Moradi F, Sedaghat S, Moradi O, Salmanabadi SA. Review on green nano-biosynthesis of silver nanoparticles and their biological activities: with an emphasis on medicinal plants. Inorg Nano-Met Chem 2020;51:133–42.
[30] Ashraf H, Anjum T, Riaz S, Naseem S. Microwave-assisted green synthesis and characterization of silver nanoparticles using Melia azedarach for the management of Fusarium wilt in tomato. Front Microbiol 2020;11:238.
[31] Wang X, Yuan L, Deng H, Zhang Z. Structural characterization and stability study of green synthesized starch stabilized silver nanoparticles loaded with isoorientin. Food Chem 2021;338:127807.
[32] Ponsanti K, Tangnorawich B, Ngernyuang N, Pechyen C. A flower shape-green synthesis and characterization of silver nanoparticles (AgNPs) with different starch as a reducing agent. J Mater Res Technol 2020;9:11003–12.
[33] Kadam J, Dhawal P, Barve S, Kakodkar S. Green synthesis of silver nanoparticles using cauliflower waste and their multifaceted applications in photocatalytic degradation of methylene blue dye and Hg2+ biosensing. SN Appl Sci 2020;2:738.
[34] Garay-Rodriguez LF, Torres-Martinez LM, Moctezuma E. Photocatalytic performance of K2Ti6O13 whiskers to H-2 evolution and CO2 photo-reduction. J Energy Chem 2019;37:18–28.
[35] Vijayan R, Joseph S, Mathew B. Costus speciosus rhizome extract mediated synthesis of silver and gold nanoparticles and their biological and catalytic properties. Inorg Nano-Met Chem 2019;85:360–5.
[36] Parveen R, Ullah S, Sgarbi R, Tremiliosi-Filho G. One-pot ligand-free synthesis of gold nanoparticles: the role of glycerol as reducing-cum-stabilizing agent. Colloid Surface Physicochem Eng Aspect 2019;565:162–71.
[37] Gholamrezaei S, Amiri M, Amiri O, Salavati-Niasari M, Moayedi H. Ultrasound-accelerated synthesis of uniform SrMnO3 nanoparticles as water-oxidizing catalysts for water splitting systems. Ultrason Sonochem 2020;62:104899.
[38] Somanathan T, Abilarasu A, Jermy BR, Ravinayagam V, Suresh D. Microwave assisted green synthesis Ce0.2Ni0.8Fe2O4 nanoflakes using calotropis gigantean plant extract and its photocatalytic activity. Ceram Int 2019;45:18091–8.
[39] Shebl A, Hassan AA, Salama DM, Abd El-Aziz ME, Abd Elwahed MSA. Template-free microwave-assisted hydrothermal synthesis of manganese zinc ferrite as a nanofertilizer for squash plant (Cucurbita pepo L). Heliyon 2020;6:e03596.
[40] Lagashetty A, Ganiger SK, Preeti RK, Reddy S, Pari M. Microwave-assisted green synthesis, characterization and adsorption studies on metal oxide nanoparticles synthesized usingFicus Benghalensisplant leaf extracts. New J Chem 2020;44:14095–102.
[41] Backes CW, Scheffer FR, Pereira MB, Teixeira SR, Weibel DE. Photosensitised degradation of organic dyes by visible light using riboflavin adsorbed on the surface of TiO_2 nanotubes. J Braz Chem Soc 2014;25:2417–24.
[42] Dal'Acqua N, Scheffer FR, Boniatti R, da Silva BVM, de Melo JV, da Silva Crespo J, et al. Photocatalytic nanostructured self-assembled poly(allylamine hydrochloride)/Poly(acrylic acid) polyelectrolyte films containing titanium dioxide-gold nanoparticles for hydrogen generation. J Phys Chem C 2013;117:23235–43.
[43] Gonçalves RV, Migowski P, Wender H, Eberhardt D, Weibel DE, Sonaglio FvC, et al. Ta_2O_5 nanotubes obtained by anodization: effect of thermal treatment on the photocatalytic activity for hydrogen production. J Phys Chem C 2012;116:14022–30.
[44] Wender H, Feil AF, Diaz LB, Ribeiro CS, Machado GJ, Migowski P, et al. Self-organised TiO_2 nanotube arrays: synthesis by anodization in an ionic liquid and assessment of photocatalytic properties. Appl Mater Interfaces 2011;3:1359–65.
[45] Strapasson GB, Scheffer FR, Cendron SW, Silva FdC, Lazzari NH, Azambuja C, et al. Visible light sensitization of TiO2/Ag/N nanostructures synthesized by microwave irradiation for oxidative degradation of organic dyes. SN Appl Sci 2020;2:543.
[46] Hejna A, Kosmela P, Formela K, Piszczyk Åu, Haponiuk JzT. Potential applications of crude glycerol in polymer technology-Current state and perspectives. Renew Sustain Energy Rev 2016;66:449–75.
[47] Backes CW, Weibel DE. Enhanced glycerol dehydration of pervaporation cross-linked PVA membranes modified by VUV/UV-C treatments. J Appl Polym Sci 2021:50723. n/a.
[48] Surendar M, Sagar TV, Raveendra G, Kumar MA, Lingaiah N, Rao KSR, et al. Pt doped LaCoO3 perovskite: a precursor for a highly efficient catalyst for hydrogen production from glycerol. Int J Hydrogen Energy 2016;41:2285–97.
[49] Mayer M. SIMNRA, a simulation program for the analysis of NRA, RBS and ERDA. AIP Conf Proceed 1999;475:541–4.
[50] Fan X, Fan J, Hu XY, Liu EZ, Kang LM, Tang CN, et al. Preparation and characterization of Ag deposited and Fe doped TiO2 nanotube arrays for photocatalytic hydrogen production by water splitting. Ceram Int 2014;40:15907–17.
[51] Mohammad R Irshidat, Mohammed HA-S, Sura S. Effect of nanoclay on expansive potential of cement mortar due to alkali-silica reaction. ACI Mater J 2015;112:801–8.
[52] Komarneni S, Li D, Newalkar B, Katsuki H, Bhalla AS. Microwave-polyol process for Pt and Ag nanoparticles. Langmuir 2002;18:5959–62.
[53] Darmanin T, Nativo P, Gilliland D, Ceccone G, Pascual C, De Berardis B, et al. Microwave-assisted synthesis of silver nanoprisms/nanoplates using a "modified polyol process. Colloids Surf, A Physicochem Eng Asp 2012;395:145–51.
[54] Schmidt B, Wetzig K. Materials analysis by ion beams. In: Ion beams in materials processing and analysis. Vienna: Springer-Verlag; 2012. p. 301–37.

[55] Stedile FC, dos Santos JHZ. Analysis and characterization of real catalysts using ion beam analysis. Nucl Instrum Methods Phys Res, Sect B 1998;136–138:1259–66.
[56] Bichinho KM, Pires GP, Stedile FC, dos Santos JHZ. Metal content determination in polymerization catalysts by direct methods. Spectrochim Acta B 2002;57:1877–84.
[57] Moreno YP, da Silva WL, Stedile FC, Cu Radtke, dos Santos JoHZ. Micro and nanodomains on structured silica/titania photocatalysts surface evaluated in RhB degradation: effect of structural properties on catalytic efficiency. Appl Surf Sci Adv 2021;3:100055.
[58] Sahu K, Bisht A, Khan SA, Sulania I, Singhal R, Pandey A, et al. Thickness dependent optical, structural, morphological, photocatalytic and catalytic properties of radio frequency magnetron sputtered nanostructured Cu2O-CuO thin films. Ceram Int 2020;46:14902–12.
[59] Cajzl J, Jeníčková K, Nekvindová P, Michalcová A, Veselý M, Macková A, et al. Creation of gold nanoparticles in ZnO by ion implantation-DFT and experimental studies. Nanomaterials 2020;10:2392.
[60] Schneidewind H, Schüler T, Strelau KK, Weber K, Cialla D, Diegel M, et al. The morphology of silver nanoparticles prepared by enzyme-induced reduction. Beilstein J Nanotechnol 2012;3:404–14.
[61] Primetzhofer D, Sytnyk M, Wagner PJ, Bauer P, Heiss W. The potential of Rutherford Backscattering Spectrometry for composition analysis of colloidal nanocrystals. Nucl Instrum Methods Phys Res, Sect B 2014;332:122–5.
[62] Lechner RT, Fritz-Popovski G, Yarema M, Heiss W, Hoell A, Schülli TU, et al. Crystal phase transitions in the shell of PbS/CdS core/shell nanocrystals influences photoluminescence intensity. Chem Mater 2014;26:5914–22.
[63] Moulder JF. Handbook of X-ray photoelectron spectroscopy: a reference book of standard spectra for identification and interpretation of XPS data. USA: Physical Electronics Division, Perkin-Elmer Corporation; 1992.
[64] Iwase A, Kato H, Kudo A. Nanosized Au particles as an efficient cocatalyst for photocatalytic overall water splitting. Catal Lett 2006;108:6–9.
[65] Ni M, Leung MKH, Leung DYC, Sumathy K. A review and recent developments in photocatalytic water-splitting using TiO_2 for hydrogen production. Renew Sustain Energy Rev 2007;11:401–25.
[66] Wu G, Chen T, Su W, Zhou G, Zong X, Lei Z, et al. H-2 production with ultra-low CO selectivity via photocatalytic reforming of methanol on Au/TiO2 catalyst. Int J Hydrogen Energy 2008;33:1243–51.
[67] Henderson MA. A surface science perspective on TiO_2 photocatalysis. Surf Sci Rep 2011;66:185–297.
[68] Zhou X, Liu G, Yu J, Fan W. Surface plasmon resonance-mediated photocatalysis by noble metal-based composites under visible light. J Mater Chem 2012;22:21337–54.
[69] Gomathisankar P, Hachisuka K, Katsumata H, Suzuki T, Funasaka K, Kaneco S. Enhanced photocatalytic hydrogen production from aqueous methanol solution using ZnO with simultaneous photodeposition of Cu. Int J Hydrogen Energy 2013;38:11840–6.